JCB Journal of Cell Biology

REPORT

Septin2 mediates podosome maturation and endothelial cell invasion associated with angiogenesis

Kerrie B. Collins, Hojin Kang, Jacob Matsche, Jennifer E. Klomp, Jalees Rehman, Asrar B. Malik, and Andrei V. Karginov

Podosomes are compartmentalized actin-rich adhesions, defined by their ability to locally secrete proteases and remodel extracellular matrix. Matrix remodeling by endothelial podosomes facilitates invasion and thereby vessel formation. However, the mechanisms underlying endothelial podosome formation and function remain unclear. Here, we demonstrate that Septin2, Septin6, and Septin7 are required for maturation of nascent endothelial podosomes into matrix-degrading organelles. We show that podosome development occurs through initial mobilization of the scaffolding protein Tks5 and F-actin accumulation, followed by later recruitment of Septin2. Septin2 localizes around the perimeter of podosomes in close proximity to the basolateral plasma membrane, and phosphoinositide-binding residues of Septin2 are required for podosome function. Combined, our results suggest that the septin cytoskeleton forms a diffusive barrier around nascent podosomes to promote their maturation. Finally, we show that Septin2-mediated regulation of podosomes is critical for endothelial cell invasion associated with angiogenesis. Therefore, targeting of Septin2-mediated podosome formation is a potentially attractive anti-angiogenesis strategy.

Introduction

Angiogenesis and vessel branching depend on the "softening" of the ECM through the directed release of proteases by endothelial cells (ECs; Potente et al., 2011). The essential requirements for protease release during angiogenesis are that it be orderly, polarized, and delivered into the subendothelial space (Spuul et al., 2016). Studies have suggested an important role for the evanescent organelles, termed podosomes, which can assemble and disassemble through as yet poorly understood mechanisms, in mediating the release of proteases (Gimona et al., 2008). Podosomes are adhesions formed within the basal membrane. They interact with matrix proteins through integrins such as $\alpha_6\beta_1$ and $\alpha_v\beta_3$ and the integrin-associated proteins talin and vinculin (Osiak et al., 2005). Podosomes have distinct organizational features. They contain a dense core composed of branched F-actin that is configured to exert pressure on the underlying plasma membrane (PM) and create invasive protrusions (van den Dries et al., 2013b). Podosomes can take on a variety of morphological configurations (Destaing et al., 2013) that appear to vary across cell types (Meddens et al., 2016). The use of such a metalloprotease "injection" system capable of localized delivery and matrix remodeling remains largely unexplored in the context of endothelial biology.

Septin2 is a member of the septin protein family expressed in many cell types (Hall et al., 2005). Septins organize to form a distinct, noncanonical cellular cytoskeleton (Zander et al., 2016). Their polymerization in vivo results in the formation of a variety of higher-order structures such as rings and cagelike networks, with Septin2 specifically binding Septin6 and Septin7 (Bridges et al., 2014; Sheffield et al., 2003). Septin2 also binds phosphoinositides (PIPs) within the PM through a conserved N-terminal stretch of basic residues referred to as the polybasic domain (Gilden and Krummel, 2010). PIP signaling is thought to be important for podosome formation (Oikawa et al., 2008). Since septins at the PM can create a diffusive barrier (Barral and Mansuy, 2007; Sharma et al., 2013a), they may function similarly in ECs to isolate a system for protease delivery into the subendothelium and thus remodel ECM.

Angiogenesis requires the invasion of endothelial protrusions into the remodeled ECM (Seano et al., 2014). Release of proteases by ECs induces enzymatic degradation of matrix proteins (Spuul et al., 2016) facilitating EC invasion, migration, and thereby vessel formation (Auerbach et al., 2003). Growth factors such as VEGF (Wang et al., 2009) and cytokines such as TGFβ (Curado et al., 2014; Varon et al., 2006) can induce podosome formation. The tyrosine kinase Src, activated downstream of VEGF and TGFβ, is an essential signaling intermediate regulating podosome assembly (Kelley et al., 2010; Boateng and Huttenlocher,

Department of Pharmacology, University of Illinois College of Medicine, Chicago, IL.

Correspondence to Andrei Karginov: Karginov@uic.edu.

https://doi.org/10.1083/jcb.201903023

2012). Although podosomes are involved in angiogenesis (Spuul et al., 2016), the sequence of events and mechanisms governing podosome-mediated angiogenesis are not defined. Here, we demonstrate the requisite role of Septin2 in regulating podosome maturation downstream of Src activation in ECs, thereby facilitating EC invasion during angiogenesis through targeted release of metalloproteases and degradation of matrix proteins.

Results

Src activation induces Septin2 localization to podosomes in ECs

We first studied the effects of Src activation on VEGF-induced podosomal matrix degradation in ECs. We observed that VEGF induced podosome function in a Src-dependent fashion (Fig. S1 A). Therefore, to study the mechanisms of Src-mediated podosome formation, we focused on events downstream of Src activation. Here, we used the allosterically regulatable rapamycin-regulated Src (RapR-Src) construct that we developed to precisely control Src activity in ECs (Klomp et al., 2016; Karginov et al., 2010, 2014). RapR-Src is an engineered protein bearing a rapamycin-sensitive allosteric switch domain. In the absence of rapamycin, RapR-Src remains catalytically inactive. The addition of rapamycin induces interaction with the coexpressed FRB protein, leading to activation of the kinase. This allows us to achieve a strict specific and temporal control of Src activity in living ECs (Klomp et al., 2016, 2019). Previous studies have shown that RapR-Src functions similarly to WT Src (Klomp et al., 2016; Chu et al., 2014; Karginov et al., 2014). We observed that Src activation induced translocation of fluorescently tagged Septin2-YFP to structures containing RapR-Src, which morphologically resembled podosome rosettes (Fig. S1, B and C; and Video 1). As mature podosomes are defined by their ability to degrade the ECM (Murphy and Courtneidge, 2011), we determined whether the observed Septin2-containing structures colocalized with matrix degradation sites. ECs were seeded onto a fluorescent gelatin substrate to form a monolayer before activating Src; functional podosomes were defined as the areas where dense F-actin structures overlapped with the quenched fluorescent gelatin signal (Martin et al., 2012), indicative of localized matrix degradation (Fig. 1 A). Upon Src activation in ECs, we observed that endogenous Septin2 was localized with multiple functional podosome configurations, including individual foci as well as rosettes (Fig. 1 A and Fig. S1, D and E).

To further characterize Septin2 localization within podosomes, we costained endogenous Septin2 with known podosome markers membrane-type matrix metalloprotease-1 (MT1-MMP; El Azzouzi et al., 2016) and the scaffold protein Tks5 (Di Martino et al., 2014). To assess their localization at a high resolution, we used Airyscan confocal microscopy. This analysis revealed that Septin2 localized around the core structure of endothelial podosomes containing MT1-MMP (Fig. 1, B and C) and Tks5 (Fig. 1, D and E). This localization of Septin2 around the border of endothelial podosomes suggests that it may be acting as a stabilizing barrier, in a manner consistent with septin function at other subcellular structures such as dendritic spines and primary cilia (Barral and Mansuy, 2007; Hu et al., 2010; Ewers et al., 2014).

Matrix metalloproteases (MMPs) are the key enzymes responsible for podosomal matrix remodeling (Cho et al., 2008; Varon et al., 2006). To assess the role of MMPs in endothelial podosome function, we performed a matrix degradation assay in the presence of MMP inhibitors. Treatment with a global inhibitor of MMP activity (GM6001; Varon et al., 2006) dramatically reduced matrix degradation by ECs (Fig. S1 F). Furthermore, treatment with an inhibitor specific for MT1-MMP (NSC405020; Kittaka et al., 2018) decreased podosome function to the same extent (Fig. S1 F), indicating that MT1-MMP is the predominant enzyme responsible for the observed Src-induced podosomal matrix degradation. Because myosin IIA has been shown to play a role in regulating different aspects of podosome biology, such as patterning in osteoclasts (Meddens et al., 2016) and turnover in macrophages (Bhuwania et al., 2012), we additionally assessed whether inhibiting its action would impede podosome function. Treatment with blebbistatin significantly attenuated matrix degradation by ECs (Fig. S1 F), which is consistent with the role of myosin observed in other cell types. These data confirm the critical functional components of the observed matrix-degrading organelles and further define these structures as endothelial podosomes.

Septins polymerize to form multimeric complexes in vivo. Septin2 binds Septin6 and Septin7 to form hexamers (Sirajuddin et al., 2007; Low and Macara, 2006), which can become octamers with the inclusion of Septin9 (Neubauer and Zieger, 2017; Soroor et al., 2019 *Preprint*). These polymers form nonpolar filaments that assemble into higher-order Septin cytoskeleton structures (Sheffield et al., 2003). We found that Septin6, Septin7, and Septin9 also localized to Src-induced podosomes characterized by the presence of the established markers cortactin and F-actin (Fig. S2, A–C). Overall, these data identify the septin cytoskeleton as a novel component of endothelial podosomes.

Physiologically occurring podosomes are also found in dendritic cells (Gawden-Bone et al., 2014). Similar matrix-degrading organelles termed invadopodia are formed in cancer cells (Wang et al., 2016; Genna et al., 2018). Though the mechanisms of podosome formation may vary across cell types, their core matrix-remodeling function remains consistent. We found that Septin2 localized to matrix-degrading organelles spontaneously formed in bone marrow–derived macrophages (BMDMs) as well as MDA-MB-231 breast cancer cells (Fig. S2, D and E). These data suggest that the septin cytoskeleton is a component of podosomes and invadopodia in a broad variety of cells.

Septin2 is required for podosomal matrix remodeling and EC invasion

We next investigated whether Septin2 was required for podosomal matrix degradation in ECs. Depletion of Septin2 expression using RNAi significantly reduced the number of cells exhibiting the podosome phenotype in response to Src activation (Fig. 2, A–D). Furthermore, Septin2 expression was required for matrix degradation stimulated by treatment with VEGF (Fig. 2 E). These data show that Septin2 mediates formation of functional podosomes downstream of both physiological stimuli and Src activation.

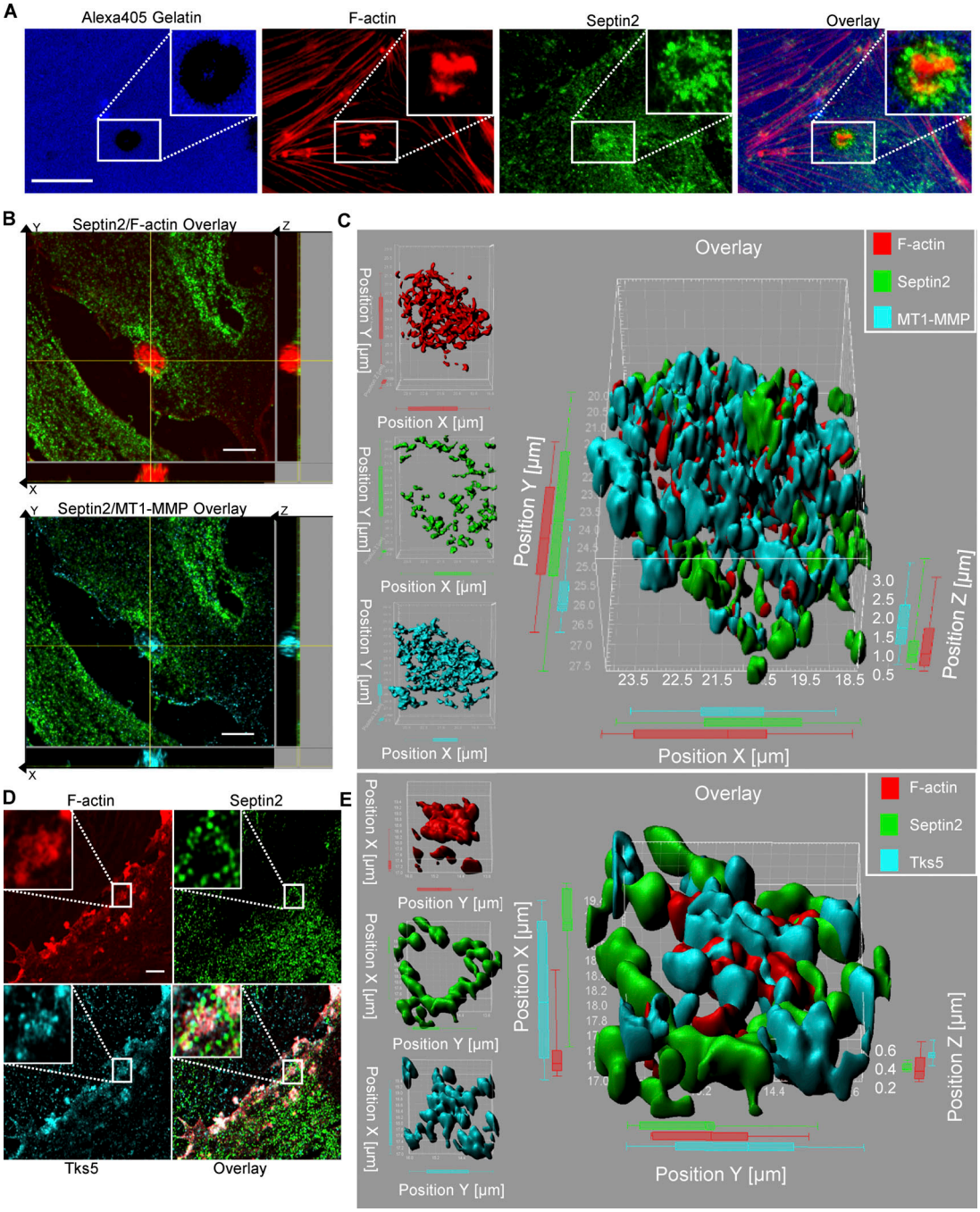

Figure 1. **Src activation induces Septin2 localization to podosomes in ECs. (A)** Confocal images showing localization of endogenous Septin2 to Src-induced functional endothelial podosome rosette (indicated by white boxes). HPAECs expressing RapR-Src were seeded onto an Alexa Fluor 405–conjugated gelatin (Alexa405-gelatin). RapR-Src was activated for 1 h. Cells were fixed and stained for F-actin and endogenous Septin2. Functional podosomes are defined as sites of dense F-actin signal colocalizing with areas where the fluorescent gelatin signal is quenched (scale bar = 10 µm). **(B and D)** Airyscan images depicting Septin2 colocalizing with known podosome markers MT1-MMP (B; scale bar = 5 µm) and Tks5 (D; zoomed images showing areas outlined with white rectangles; scale bar = 3 µm). Cells were prepared as in A, seeded onto unlabeled gelatin substrate, and fixed and stained after 0.5 h of RapR-Src activation. **(C and E)** Imaris image analysis software was used to create a 3D surface rendering of endogenous Septin2 colocalizing with MT1-MMP (C) and Tks5 (E) in endothelial podosomes.

Because we observed the localization of Septin6 and Septin7 to podosomes (Fig. S2, A and B), we sought to determine whether they were also important for regulation of endothelial podosome function. Similar to Septin2, depleting Septin6 and Septin7 expression also significantly decreased podosomal matrix degradation (Fig. S2, F–H), suggesting that the Septin2/Septin6/Septin7 hexamer regulates podosome function.

Previous studies have demonstrated that depleting one member of the septin protein family can alter the expression of others (Peng et al., 2002). We therefore looked at Septin2,

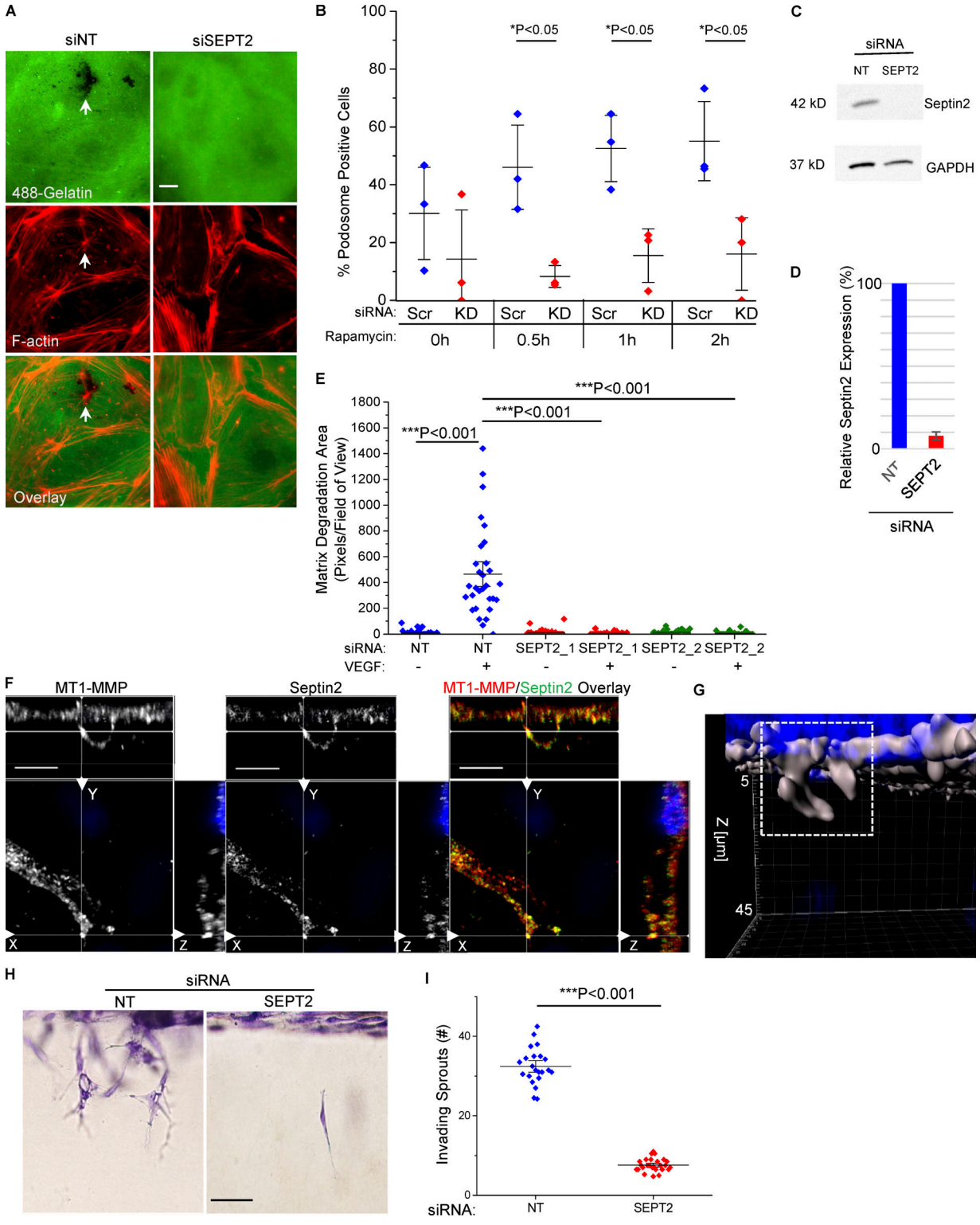

Figure 2. **Septin2 expression is required for podosome-mediated matrix degradation and invasion in vitro. (A–D)** Effect of Septin2 downregulation on the ability of ECs to form functional podosomes in response to Src activation. HPAECs were treated with 35 nM siRNA targeting Septin2 (SEPT2) or NT scramble control for 48 h before being seeded onto Alexa488-gelatin and transduced with adenoviral constructs expressing RapR-Src and FRB. After an additional 24 h, RapR-Src was activated for 30 min, 1 h, and 2 h with rapamycin (500 nm), and cells were fixed and stained for F-actin. **(A)** Representative epifluorescence images of HPAECs 30 min following Src activation. White arrows indicate functional podosomes defined as in Fig.1 A (scale bar = 50 µm). **(B)** Percentage of HPAECs displaying the matrix-degrading podosome phenotype before (0 h) and after activation of Src (time points are indicated). For each condition, a minimum of 10 fields of view were analyzed per experiment. Data show results from three independent experiments. KD, knockdown. **(C)** Western blot analysis displays downregulation of endogenous Septin2 with respect to GAPDH loading control used in A. **(D)** Average relative Septin2 expression normalized to scramble control (n = 3). Error bars represent standard deviation. **(E)** Role of Septin2 in VEGF-stimulated matrix degradation. Septin2 expression

was downregulated as in A. Cells were deprived of VEGF for 48 h, serum starved in for 2 h, and then seeded onto Alexa405-gelatin. Total matrix degradation was measured after 5 h of VEGF stimulation. At least 10 fields of view per condition were analyzed from three independent experiments. Individual data points are shown around mean value ± SE (whiskers). **(F and G)** Septin2 localizes to invading sprouts in vitro. **(F)** HPAECs were seeded atop a 3D collagen matrix and stimulated using growth factor/S1P mix for 20 h. Following stimulation, cells were fixed and stained for endogenous Septin2 and MT1-MMP (confocal images, scale bar = 10 µm). **(G)** Representative 3D surface rendering of an invading sprout shown in F created with Imaris (indicated by white box; DAPI-stained nuclei represented in blue). **(H and I)** Effect of Septin2 downregulation on cell invasion. Septin2 expression was downregulated as in A and invasion was stimulated as in F. Following stimulation, cells were fixed and stained with toluidine blue. **(H)** Representative images showing cell invasion (lateral view of invading sprouts; scale bar = 0.15 mm). **(I)** Quantification of invading sprouts. Each data point represents an average of two to four fields per well imaged over three independent experiments. Data are represented as mean ± SE. Significance was determined using a two-sample *t* test (comparisons indicated by lines; B, E, and I).

Septin6, and Septin7 expression levels in response to treatment with siRNA targeting their binding partners within the Septin2/Septin6/Septin7 hexamer. Our results indicated that expression of Septin2, Septin6, and Septin7 each significantly decreased in response to this treatment (Fig. S2 I). However, the effect varied between septins, and in most cases, expression did not decrease by >50%. Thus, our results are in agreement with previously reported observations.

The association of Septin9 with Septin2/Septin6/Septin7 hexamers can affect the stability of higher-order septin structures and cellular functions (Kim et al., 2011). We therefore investigated whether Septin9 expression was required for podosome function. Despite the fact that Septin9 localized to Src-induced podosome foci (Fig. S2 C), decreasing Septin9 expression using RNA interference had no significant effect on podosomal matrix degradation (Fig. S2, J and K). Taken together, these results indicated a role for the Septin2/Septin6/Septin7 hexamer, independent of Septin9, in regulating podosomal matrix degradation in ECs.

As matrix degradation is required for invasion of ECs into a 3D ECM, we assessed the effect of Septin2 downregulation on EC invasion (Kang et al., 2008). Staining of ECs in a 3D collagen matrix demonstrated colocalization of Septin2 and MT1-MMP in the invading sprouts (Fig. 2, F and G). Additionally, we observed that downregulation of Septin2 expression significantly reduced the total number of invading endothelial sprouts (Fig. 2, H and I; and Fig. S3 A). We next assessed whether Septin2-mediated podosome function was required for EC invasion, which is associated with angiogenesis. These studies were performed by implanting Matrigel plugs containing Septin2-depleted ECs into athymic nude mice (Fig. 3, A and B). We observed severely defective blood vessel formation in plugs containing Septin2-depleted ECs compared with control cells (Fig. 3 C). The vessels lacked characteristic organization of ECs and were not perfused by erythrocytes (Fig. 3, C–E). Staining for human specific CD31 in Matrigel plug sections (Fig. 3 F) demonstrated that the injected ECs were associated with the blood-perfused vessels within the plugs. Taken together, these results demonstrate the requirement for Septin2 in mediating the EC invasion that accompanies the formation of perfused blood vessels in vivo.

Invasion of ECM by ECs and the subsequent formation of blood vessels comprises three main steps: podosomal matrix degradation, migration, and network formation. Our data demonstrated that Septin2 mediates matrix degradation (Fig. 2, A–E). We also sought to determine if Septin2 is required for EC migration and network formation. To eliminate the dependence on matrix degradation, we performed these assays in a 2D format as described in previous publications (Auerbach et al., 2003; Kang et al., 2019; Guo et al., 2014). Downregulation of Septin2 expression had no effect on EC migration in a 2D wound healing assay (Fig. S3, B and C) or their capacity to form branched networks in a 2D culture (Fig. S3, D and E).

Focal adhesions share many components with podosomes (Hoshino et al., 2012; van den Dries et al., 2013a), and they also mediate interactions with ECM, affecting cellular motility, albeit without performing matrix degradation (Burridge and Guilluy, 2016; Block et al., 2008). We therefore next assessed whether Septin2 is also required for focal adhesion formation. Our results indicated that Septin2 depletion had very little impact on the total number of focal adhesions formed (Fig. S3 F). Taken together, these results indicate that the primary role of Septin2 in ECs is to mediate podosome function and thereby facilitate the initial step of angiogenic invasion.

Septin2 recruitment into nascent podosomes follows the mobilization of precursor proteins

Initial assembly of nascent podosome structures, their maturation into matrix-degrading organelles, and eventual turnover are distinctly regulated phases comprising the life cycle of these dynamic adhesions (Boateng and Huttenlocher, 2012). Initiation and maturation of podosomes are multistep events (Destaing et al., 2008), mediated in large part by cytoskeletal networks. Actin polymerizes during initial precursor assembly, drives invasion of mature podosomes into the ECM, and joins individual podosome foci into higher-order networks (Linder and Wiesner, 2016; Luxenburg et al., 2012; Destaing et al., 2013). Thus, we first assessed whether Septin2 expression is required for the formation of F-actin foci, which is characteristic of initial podosome assembly (Oikawa et al., 2008). We found that Src-mediated F-actin focus formation was not affected by the downregulation of Septin2 expression, indicating that it does not control nascent podosome initiation (Fig. 4 A). We next investigated the kinetics of Septin2 localization to nascent podosome foci relative to the arrival of the known precursor proteins F-actin and Tks5 using live cell imaging. We found that Tks5 arrived at nascent podosomes 30 s before F-actin (on average; Fig. 4, B, C, and F), consistent with the role of Tks5 as a scaffold protein initiating early actin-mediated podosome formation (Boateng and Huttenlocher, 2012; Seals et al., 2005; Gimona et al., 2008). However, Septin2 arrived later (around 2 min after Tks5 on average; Fig. 4, D–F), indicating its role during the late stage of podosome maturation. Taken together, these results suggest that Septin2 is required to mediate the transition of nascent podosome foci into mature matrix-degrading organelles.

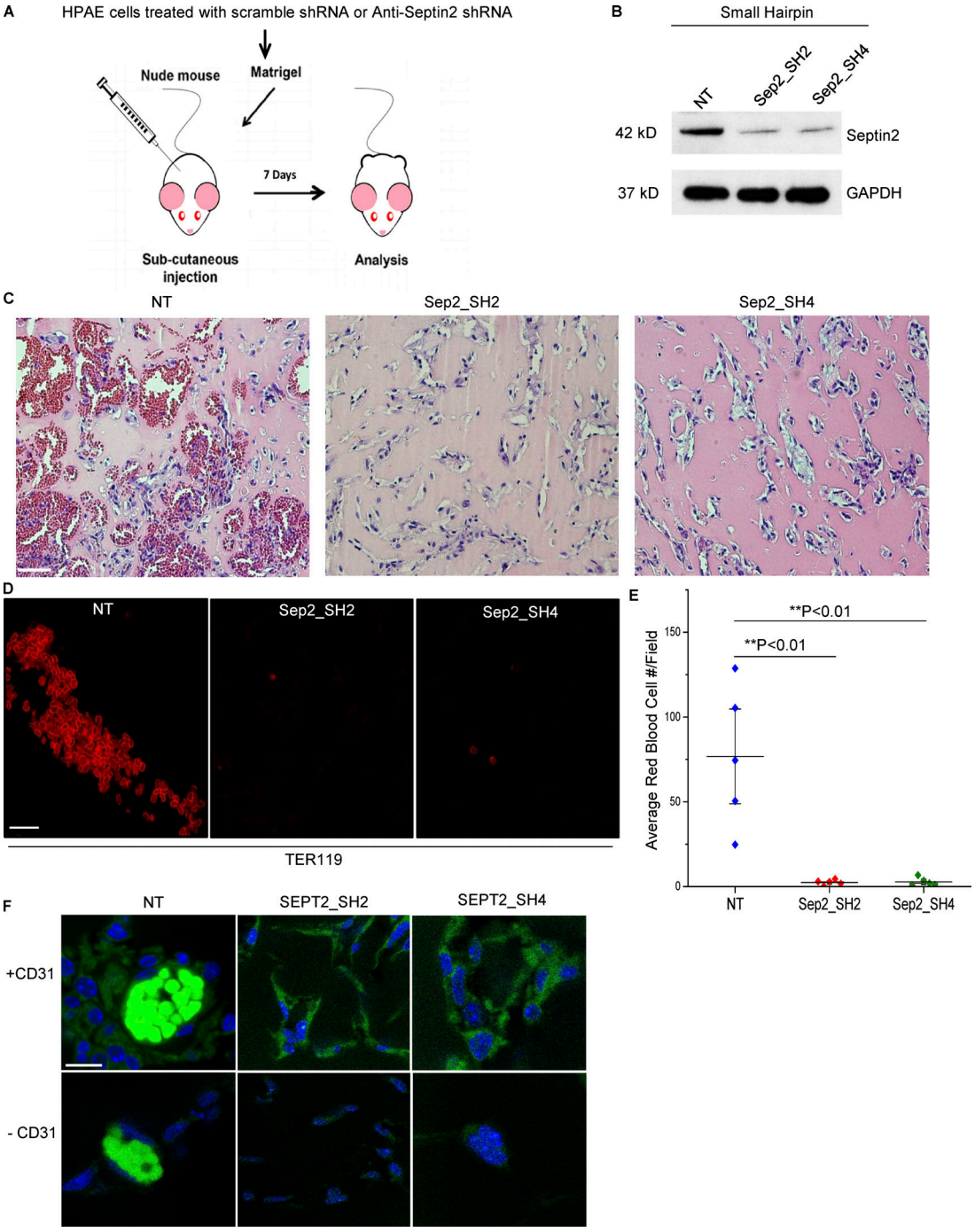

Figure 3. **Septin2 is required for perfused blood vessel formation in vivo. (A)** Schematic of the in vivo assay. HPAECs were transduced with lentiviral constructs expressing either control shRNA (NT) or two different shRNAs targeting Septin2 (Sep2-SH2 and Sep2-SH4). Equal numbers of cells from each condition were mixed with Matrigel, subcutaneously injected into athymic nude mice, and harvested 7 d later for analysis of blood vessel formation. **(B)** Western blot analysis displays downregulation of endogenous Septin2 with respect to GAPDH loading control at time of injection. **(C–E)** Analysis of Matrigel plugs. Extracted Matrigel plugs were paraffin embedded, and sections were either labeled with hematoxylin and eosin staining to visualize vessel morphology (C; scale bar = 30 mm) or immunostained with antibody targeting mouse erythrocytes (TER119; D; confocal microscopy; scale bar = 20 µm). **(E)** Average number of red blood cells per field of view were quantified to assess the formation of functionally perfused vessels. Each data point represents the average of four fields of view taken from each of five separate Matrigel plugs per condition and implanted in five separate mice (n = 5). Data are shown as the mean ± SE. Significance was determined using a two-sample t test. **(F)** Confocal images depicting the presence of HPAECs in Matrigel plug slices from each condition. Slices were stained with DAPI (blue) and human specific anti-CD31 primary antibody (+CD31, green; scale bar = 10 µm). Negative control (–CD31) was performed to reveal nonspecific binding of secondary antibody, and autofluorescence signal (bright green signal in NT samples) is due to autofluorescence of erythrocytes.

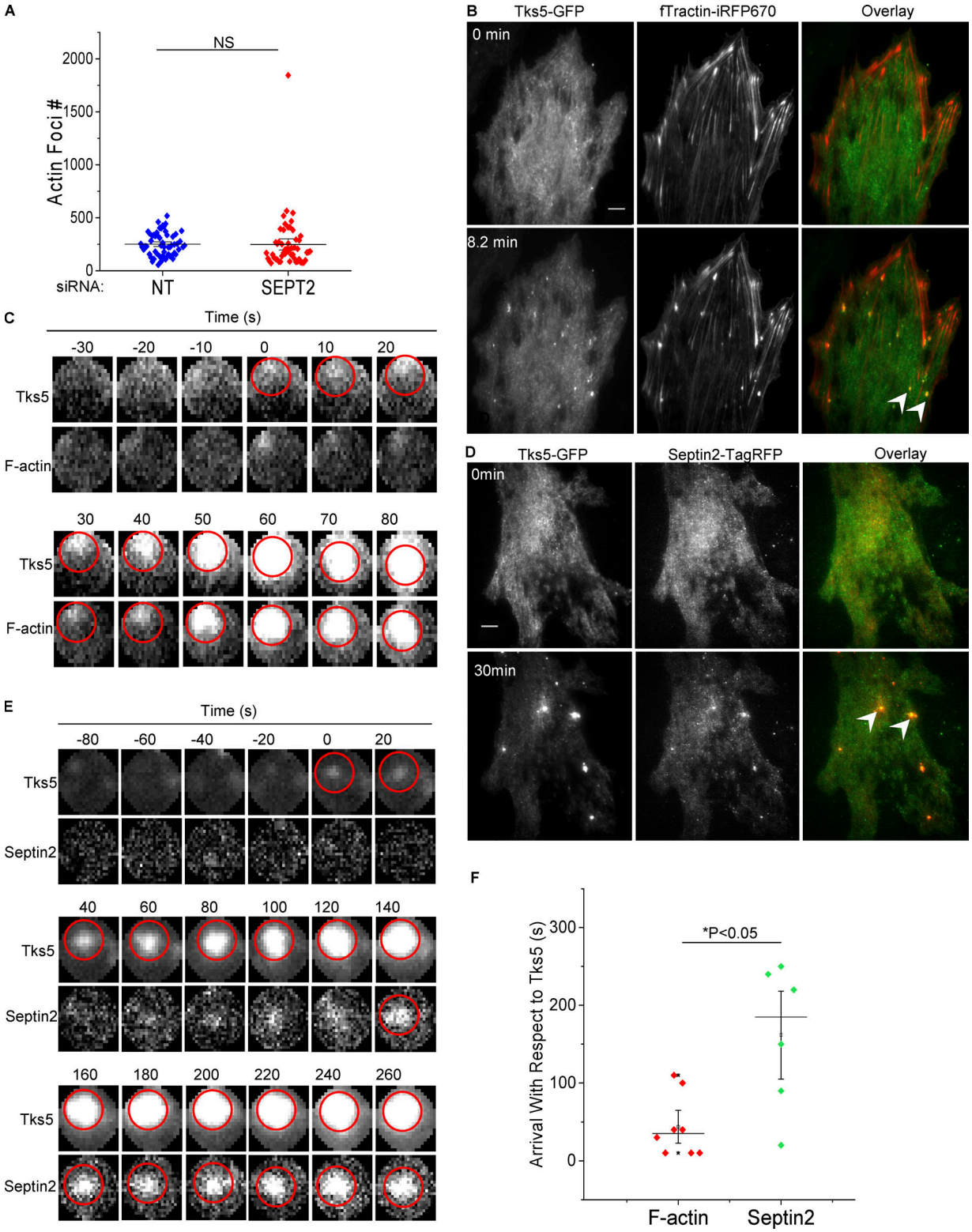

Figure 4. **Septin2 is recruited into nascent podosomes following assembly of the precursor complex. (A)** Src-mediated actin rearrangement in the presence and absence of Septin2. HPAECs were treated with siRNA for Septin2 (SEPT2) or control siRNA (NT) for 72 h. Cells were transduced with adenoviral constructs for expression of RapR-Src and FRB. Cells were fixed and stained for F-actin following 0.5 h Src activation. Epifluorescence images were analyzed using an ImageJ "invadopodia colocalization" macro to count F-actin foci. Data were collected from five independent experiments (n = 5), with each dot representing one field of view. Error bars represent SE. Statistical significance was determined using a two-sample t test. **(B–E)** HPAECs coexpressing RapR-Src with Tks5-GFP and fTractin-iRFP670 (F-actin marker; B) or Tks5-GFP and Septin2-tagRFP (D) were imaged live following Src activation (using total internal reflection fluorescence microscopy; scale bar = 8 µm). Representative time-lapse images (C and E) show the order of arrival of Septin2 and F-actin relative to the known podosomal precursor Tks5 (Tks5 arrival time = 0 s). Arrival of the protein was detected using Invadopodia Tracker V3 plugin for ImageJ software.

Time of arrival is marked by appearance of the red circle. Arrowheads indicate podosome foci. **(F)** Arrival times of F-actin and Septin2 with respect to Tks5. Data show arrival times of each protein (n = 8 for F-actin and n = 6 for Septin2) with respect to Tks5 ± SE, with each dot representing an individual focus. Statistical significance was determined using a Student's t test for pairwise comparison of F-actin with Septin2.

Septin2 residues, which mediate PIP binding, are critical for regulation of endothelial podosome function

Phospholipids play an important role in podosome formation (Hoshino et al., 2013). Src activates PI3 kinase, stimulating production of phosphoinositide (3,4,5) trisphosphate (Klomp et al., 2016) and the subsequent production of phosphoinositide (3,4) bisphosphate (Oikawa et al., 2008; Symons, 2008). Synthesis of phosphoinositide (3,4) bisphosphate induces association of the podosome scaffolding protein Tks5 with the PM, leading to stabilization of early podosomes (Hoshino et al., 2013). Septins associate with the PM and create diffusive barriers, which promote sequestration of proteins and isolate distinct signaling platforms (Schmidt and Nichols, 2004; Hu et al., 2010; Sharma et al., 2013a). To assess whether Septin2 is membrane proximal in podosomes and to further define the details of its localization within podosomal architecture, we analyzed Septin2 distribution relative to β_3 integrin, a transmembrane protein and a known podosome marker (Chellaiah, 2006). We observed that endogenous Septin2 localized to the basolateral membranes of ECs, as evidenced by its overlap with β_3 integrin in a Z axial distribution (Fig. 5, A–C). Our results also demonstrated that Septin2 localizes around the β_3 integrin in endothelial podosomes.

Septin2 binds PIPs, PtdIns$_{4,5}$P$_2$, and PtdIns$_{3,4,5}$P$_3$ in the PM through the conserved N-terminal stretch of basic residues, polybasic domain (Casamayor and Snyder, 2003; Damalio et al., 2013; Gilden and Krummel, 2010). Thus, we next evaluated whether Src activation induced colocalization of PIPs with Septin2 and if this Septin2-PIP association was required for podosome maturation. To measure PIP accumulation in living ECs, we used a sensor composed of the PH domain of Akt fused to Venus fluorescent protein (Klomp et al., 2016; Rowland et al., 2012). We observed that activation of Src induced the accumulation of Septin2 and PIPs at the same site (Fig. 5 D). To establish the role of Septin2 binding to PIPs in mediating podosome formation, we used a Lys33Ala/Lys34Ala mutant of Septin2 (K33,34A) with a diminished capacity for PIP binding (Zhang et al., 1999). WT mouse Septin2 or its Lys33Ala/Lys34Ala mutant was expressed in human ECs lacking endogenous Septin2. We observed that exogenous expression of WT Septin2 rescued Src-induced podosomal matrix degradation (Fig. 5 E and Fig. S4). However, expression of the Lys33Ala/Lys34Ala mutant failed to restore podosome function, indicating that the interaction of Septin2 with PIPs in the PM was required for the formation of mature matrix-degrading podosomes.

To date, the formation and maturation of matrix-degrading organelles has been best characterized in cancer cells. Little is known about the mechanism governing endothelial podosome formation and its role in mediating angiogenesis. The present study describes the regulation of endothelial podosomes by the septin cytoskeleton as a requirement for EC invasion. Taken together, our studies suggest a mechanism whereby Septin2 associates with PIPs at the basolateral endothelial PM to generate a stable barrier around Src-induced podosomes, ensuring containment of critical components and maturation of nascent foci into functional organelles (Fig. 5 F). These results are consistent with the postulated role for septins in partitioning subcellular structures. Previous studies have demonstrated the role of Septin2 in controlling the distribution of membrane-bound proteins and receptors (Schmidt and Nichols, 2004) and the formation of a ringlike septin cytoskeleton structure at the base of primary cilia in mammalian cells, which separates the ciliary membrane from the PM (Hu et al., 2010). Septin2 has also been shown to regulate store-operated calcium entry by forming a diffusive barrier around STIM1/Orai channels and stabilizing the clusters (Sharma et al., 2013a). Other cytoskeletal networks, including microtubules and intermediate filaments, are thought to contribute to podosome maturation via delivery of podosome component proteins (Wiesner et al., 2010; Schoumacher et al., 2010). Interestingly, septins interact with microtubules, F-actin, and myosin (Spiliotis, 2018; Schmidt and Nichols, 2004; Bowen et al., 2011; Joo et al., 2007), and these interactions could potentially mediate alternative aspects of podosome biology such as delivery of component proteins, patterning, or turnover.

Materials and methods

Antibodies and chemical reagents

Antibodies used

Antibodies used were as follows: Anti-Septin2 (Cat# 07–1813; Millipore for Western blot; and Cat# HPA018481; Sigma-Aldrich for IF); additional anti-Septin2 antibody used for immunofluorescence was a generous gift from Dr. Elias Spiliotis (Drexel University, Philadelphia, PA; Spiliotis et al., 2008; Fig. 1 A), anti-Septin9 (Cat# sc-293291; Santa Cruz), anti-Septin6 (Cat# sc-514806; Santa Cruz for Western blot), anti-SEPT7 (Cat# ab175229; Abcam for Western blot), anti-Cortactin (Cat# 05–180; Millipore), anti-MMP14 (MT1-MMP; Cat# MAB3328; Millipore), anti-Tks5 (fish, G-7; Cat# sc-376211; Santa Cruz), anti-FAK (Cat# 610087; BD PharMingen), anti-GAPDH (Cat# AM4300; Ambion), anti-mCherry (Cat# 5993–100; BioVision), FITC-conjugated AffiniPure Donkey anti-Rabbit IgG (H+L; Cat# 711–095-152; Jackson Immunoresearch), Rhodamine Red-X AffiniPure Donkey Anti-Rabbit IgG (H+L; Cat# 711–295-152; Jackson Immunoresearch), Alexa Fluor 647 AffiniPure Donkey Anti-Rabbit IgG (H+L; Cat# 711–605-152; Jackson Immunoresearch), Goat Anti-Mouse IgG1 Secondary Antibody (Atto 488; Cat# LS-C209452; LSBio), Purified Rat Anti-Mouse TER-119 rat anti-mouse erythrocyte (Cat# 550565; BD PharMingen), and IHCPlus PECAM-1/CD31 Antibody Monoclonal (Cat# LS-B3446; LSBio).

Chemical reagents used

Chemical reagents used were as follows: Alexa Fluor 647 phalloidin (Cat# A22287; Thermo Fisher), Alexa Fluor plus 405 phalloidin (Cat# A30104; Thermo Fisher), D-*erythro*-sphingosine-1-phosphate

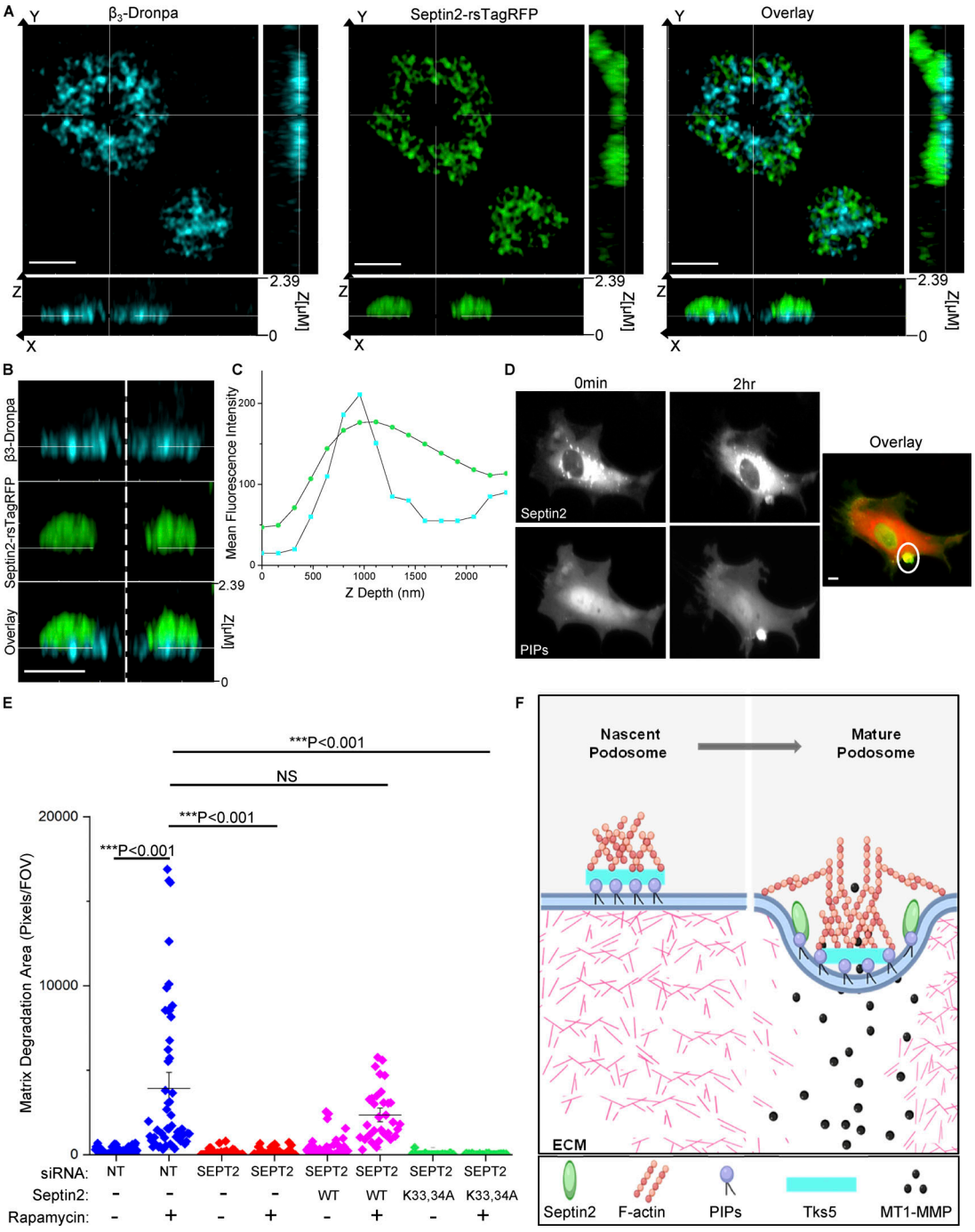

Figure 5. **Septin2 binding to PIPs mediates podosome function. (A–C)** Substrate-proximal localization of Septin2 in podosomes depicted by Airyscan confocal imaging. HPAECs expressing Septin2-rsTagRFP and β_3-Dronpa, transduced with adenoviral constructs for expression of RapR-Src and FRB and fixed following 0.5 h of Src activation. **(A)** Orthogonal view of Src-induced rosette (scale bar = 3 µm). **(B)** Zoomed-in view of orthogonal slice as in A (scale bar = 2 µm). **(C)** Depth profile of β_3 integrin (blue) and Septin2 (green) localization in the Z axial direction from the rosette depicted in A. **(D)** HPAECs expressing Septin2-mCherry (top) and a Venus-fused PIP binding probe (bottom) were imaged live using widefield illumination before and after Src activation (scale bar = 5 µm). Colocalization of Septin2 (red) and PIP binding probe (green) is indicated by the white circle in the overlay panel. **(E)** Rescue of matrix degradation by exogenous expression of Septin2. HPAECs were treated with siRNA for Septin2 (SEPT2) or control siRNA (NT) for 72 h. Cells were transduced with adenoviral constructs for expression of RapR-Src and FRB and with lentiviral constructs for expression of either WT mouse Sept2-mCherry or its mutant (Lys33Ala/Lys34Ala, K33,34A). Total matrix degradation was measured from at least 10 fields of view per condition from three to five independent experiments. Individual data points are shown around mean value ± SE (whiskers). Significance was determined using a two-sample *t* test (comparisons indicated by lines; FOV, field of view). **(F)** Model depicting the role of Septin2 in podosome maturation. Podosome initiation (left panel): Tyrosine kinase Src is activated downstream of growth factor signaling. Src signals through multiple intermediates including PI3K, which generates PIPs. These PIPs localize to sites of podosome adhesion and bind scaffolding protein Tks5. Podosome maturation (right panel): Septin2 localizes to podosomes downstream of Src activation and binds PIPs via its polybasic domain. The Septin cytoskeleton creates a confinement border around the adhesion ring, allowing for maturation and localized matrix degradation (image created with BioRender).

(Cat# 860492; Avanti Polar Lipids), normal donkey serum (Cat# 017-000-121; Jackson Immunoresearch), rapamycin (Cat# R5000; LC Laboratories), puromycin dihydrochloride (Cat# P-600-100; Gold Biotechnology), insulin (Cat# I-1882; Sigma-Aldrich), human holo transferrin (Cat# T-4132; Sigma-Aldrich), sodium selenite (Cat# 5–5261; Sigma-Aldrich), FA-free BSA (Cat# A8806; Sigma-Aldrich), oleic acid (Cat# O7501; Sigma-Aldrich), collagen I, bovine (Cat# A10644-01; GIBCO BRL), Alexa Fluor 405 NHS Ester (succinimidyl ester; Cat# A30000; Thermo Fisher), Oregon Green-488–conjugated gelatin (Cat# G13186; Thermo Fisher), ascorbic acid (Cat# A4034; Sigma-Aldrich), and basic fibroblast growth factor (Cat# 234-FSE; R&D Systems), VEGF165, human (Cat# 1150–05-10; Goldbiotech), GM6001 MMP Inhibitor (Cat# CC1000; Sigma-Aldrich), MT1-MMP inhibitor, NSC405020 (Cat# 444295; Sigma-Aldrich), blebbistatin (Cat# 2406–1; BioVision), and saracatinib (Cat# sc-45364607; Santa Cruz).

Experimental model and subject detail

Cell culture, transfection, and transduction

All human pulmonary arterial endothelial cells (HPAECs; Cat# CC-2530; Lonza) were grown in EGM-2 BulletKit (Cat# CC-2162; Lonza) with 10% FBS at 37°C and 5% CO_2. Cells obtained from Lonza at P3 were amplified and frozen at P5. Experiments were performed on cells from passages 6 to 9. Plastic growth surfaces were coated with 0.2% gelatin. Glass growth surfaces were coated with 0.2% gelatin and 5 mg/ml fibronectin. Cytofect endothelial transfection reagent (Cat# TF101K; Cell Applications) was used for transfecting HPAECs seeded at a confluency of 75% to 80% at time of transfection according to the manufacturer's protocol. Experiments were performed 16–24 h after transfection. For lentiviral infections, cells were infected for at least 72 h preceding experiments. Cells were exposed to adenovirus for 16–24 h before experiments. All HEK293T cells (Cat# ATCC CRL-3216) and MDA-MB-231 cells (a generous gift from Dr. Jan Kitajewski, University of Illinois at Chicago, Chicago, IL) were grown in DMEM (Cat# 15–013-CV; Mediatech) with 10% FBS at 37°C in 5% CO_2. All BMDMs were extracted from male mice (C57BL/6J, 18 wk/male; The Jackson Laboratory) and grown in RPMI1640 (11875–093)+10%FBS+P/S+ 10% L929 cell supernatant at 37°C in 5% CO_2 for 5 d to differentiate before experiments.

In vivo Matrigel plug angiogenesis assay

Assay was performed in athymic nude mice (Envigo) as previously described (Marsboom et al., 2016). Mice were males, aged 6–8 wk at the time of experiment. Two separate lentiviruses expressing small hairpins targeting Septin2 (SH2 and SH4) were used to downregulate Septin2 expression in HPAECs. Transduction particles were purchased from Sigma-Aldrich (Cat# SHCLNV for SH2 Clone ID TRCN0000062156 and SH4 Clone ID TRCN0000420619; scrambled nontargeting [NT] control, Cat# SHC002V). Cells were transduced with lentivirus expressing one of two small hairpins targeting Septin2 or an NT scramble control. Puromycin (Cat# P-600-100; Gold Biotechnology) at 1 µg/ml was used to select transduced cells. 1,000,000 cells per plug were mixed with growth factor–depleted Matrigel (Cat# 356234; Corning), injected subcutaneously into the abdomen of male mice (6–8 wk old), and collected 7 d later. One plug per condition was implanted in the abdomen of five separate mice. Plugs were paraffin embedded, sectioned into 10-µm slices, and stained either using hematoxylin and eosin or immunostained using TER-119 rat anti-mouse erythrocyte targeting antibody (Cat# 550565; BD PharMingen) to assess vessel perfusion or human-specific CD31 primary antibody to assess whether vessel-forming cells present in plugs were HPAECs IHCPlus PECAM-1/CD31 Antibody Monoclonal (Cat# LS-B3446; LSBio). Hematoxylin and eosin–stained samples were imaged using an Olympus BX51 microscope under transmitted light using 20× Plan N objective (NA 0.4). Samples stained for mouse red blood cells (Fig. 3 D) and human ECs (Fig. 3 F) were imaged using a Zeiss LSM 710 META microscope (63× oil objective, NA 1.46). Signal was unmixed using Zen 2012 SP1 Image Analysis software in order to resolve the signal in both cases. ImageJ cell counter (https://imagej.nih.gov/ij/plugins/cell-counter.html; Kurt De Vos) was then used to quantify the number of red blood cells per field of view. Four fields of view were analyzed for each plug to determine the average value from each mouse. Pairwise statistical comparisons between Septin2 and scramble control shRNA-treated cells were made using a Student's *t* test. P values <0.05 were considered to be significant (Fig. 3, D and E). Mice were housed in the University of Illinois Animal Care Facility under pathogen-free conditions in accordance with institutional guidelines.

Method details

Plasmids and viral constructs

All adenoviral constructs for expression of RapR-Src-Cerulean, RapR-Src-as2-Cerulean were previously described and produced in collaboration with Dr. Jody Martin at the Vector Core Facility of the University of Illinois at Chicago (Klomp et al., 2016). Additional amplification of RapR-Src-as2-Cerulean and GFP(Y66S)-FRB was performed by Viraquest, Inc., in collaboration with Ronald E. Haskell. Adenoviral constructs for expression of mCherry-FRB and GFP(Y66S)-FRB were generated from the previously described GFP-FRB adenoviral construct (Klomp et al., 2016) using site-directed mutagenesis PCR as previously described (Karginov and Hahn, 2011). The Y66S mutation renders GFP colorless. pkSeptin2-YFP plasmid was a generous gift from Dr. Ian Macara (Vanderbilt University, Nashville, TN). Septin6-GFP and Septin7-GFP plasmids were a generous gift from Dr. Elias Spiliotis. Septin2-Tag-RFP, Septin2-mCherry, and Septin2-K33,34A-mCherry were created from pkSeptin2-YFP using modification of site-directed mutagenesis (Karginov and Hahn, 2011). Septin2-rsTagRFP plasmid was created by amplifying the rsTagRFP gene from the pcDNA3-ER-rsTagRFP construct (Hertel et al., 2016; a generous gift from Dr. Gary Mo, University of Illinois at Chicago, Chicago, IL; #87620; Addgene). rsTagRFP was then subcloned into the previously described Septin2-mCherry construct using a modification of site-directed mutagenesis (Karginov and Hahn, 2011). β_3-Dronpa construct was created by amplifying the dronpa gene from pcDNA3-Dronpa-DEVD-TagRFPT (a generous gift from Dr. Gary Mo; #87704; Addgene) and subcloning this gene into PBLY100-GFP plasmid bearing β_3 integrin (a generous gift from Dr. Rudolph L. Juliano, University of North Carolina, Chapel Hill, NC) using

modified site-directed mutagenesis (Karginov and Hahn, 2011). The PH-Akt-Venus construct was previously described (Klomp et al., 2016). TKS5-GFP plasmid was a gift from Dr. Sara A. Courtneidge (Oregon Health and Science University, Portland, OR). F-tractin gene was amplified from previously described fTractin-tdTomato construct (Schell et al., 2001) and subcloned into iRFP670-N1 plasmid (a gift from the laboratory of Dr. Vladislav Verkhusha, Albert Einstein College of Medicine, Bronx, NY) using modification of site-directed mutagenesis (Karginov and Hahn, 2011) to create fTractin-iRFP670. To generate lentiviral constructs, Septin2 and Septin2 K33,34A mutant genes were amplified using PCR primers encoding NotI and BsiWI restrictions sites and cloned into pLeGOiV-2 vector (plasmid #27344; Addgene) using NotI and BsrGI restriction sites. Lentivirus production was performed as previously described (Gong et al., 2017).

Downregulation of Septin expression using siRNA

Cells were transfected using either Dharmafect or GeneSilencer transfection reagent for 72 h before experiments. Cells were transfected using 35 nM siRNA. Septin2 was downregulated using a pool of four individual siRNAs (knockdown experiments depicted in Fig. 2 and Fig. S3 A; Cat# D-010614-05, Cat# D-010614-03, Cat# D-010614-21, Cat# D-010614-20; Dharmacon), a pool of two individual siRNAs (experiments depicted in Fig. 4 A; Fig. 5 E; Fig. S3, B–E; and Fig. S4; Cat# D-010614-05 and Cat# D010614-03; Dharmacon), or two individual siRNAs (Fig. 2 E and Fig. S3 F; Cat# D-010614-05 and Cat# D010614-03; Dharmacon). Septin 6 was downregulated using two individual siRNA (Fig. S2, F and H; Oligo# 3021663579-000050 and Oligo# 3021663579-000020; Sigma-Aldrich). Septin7 was downregulated using two individual siRNA (Fig. S2, G and H; Oligo# 3021663579-000170 and Oligo# 3021663579-000140; Sigma-Aldrich). Septin9 was downregulated using two individual siRNA (Fig. S2, J and K; Cat# D-006373-06 and Cat# D-006373-02; Dharmacon).

Immunofluorescence

Cells were fixed for 15 min at room temperature using 4% paraformaldehyde and permeabilized using 0.5% Triton-X. Blocking was performed for 30 min at room temperature in 3% BSA and 20% donkey serum. Samples were incubated with primary antibody (1:100) in 10% donkey serum and 1.5% BSA for 1 h at room temperature and in secondary antibodies (1:200) for 1 h at room temperature. Alexa Fluor 647 phalloidin (1:200; Cat# A22287; Thermo Fisher) and Alexa Fluor plus 405 phalloidin (Cat# A30104; Thermo Fisher) were added to samples either with secondary antibody or directly after blocking at room temperature for 0.5 h in samples where only F-actin was being labeled.

Wound healing assay

Migration was measured using a scratch wound healing assay as previously described (Liang et al., 2007). HPAECs were seeded on glass coverslips coated in 0.2% gelatin and fibronectin (5 mg per liter). Coverslips were mounted in an Attofluor cell chamber (Cat# A78-16; Invitrogen). Images were collected using Olympus VivaView Incubator/Fluorescence Microscope with 40× air objective (equivalent to UPLSAPO40X, NA 0.95) under transmitted light at 37°C in 5% CO_2. MRI wound healing plugin for ImageJ Image Analysis software was used to measure the distance migrated by cells. The distance was measured at 5 to 10 positions for each field of view and averaged. The distance measured for each sample was then normalized by the average distance for scramble control in the same experiment. Results from three or four independent experiments were expressed as normalized distance traveled. Statistical significance was determined using a Student's *t* test for pairwise comparison between conditions.

EC network formation

Assay was performed as previously described (Han et al., 2012; Kang et al., 2019; Auerbach et al., 2003; Guo et al., 2014). Cells were seeded in a 96-well plate atop growth factor–depleted Matrigel for 2 h. Images were captured using Olympus BX51 fluorescence microscope under transmitted light using UPlan FLN 4× objective (NA 0.13). Angiogenesis Analyzer module (Carpentier, 2012) for ImageJ software was used to create a mask of branched networks and quantify the number of branches, branch length, and number of segments. For each of three independent experiments, one field of view was analyzed per well for a total of three wells per condition (Fig. S3, D and E).

Invasion into 3D collagen matrix

Assay was performed as previously described (Kwak et al., 2012). Aptitude for invasion was compared in cells with downregulated Septin2 expression versus scramble control cells. HPAECs were seeded onto a 3D collagen matrix at a density of 40,000 cells per well in a 96-well plate and allowed to invade for 24 h, fixed with 3% glutaraldehyde in PBS, and stained with 0.1% toluidine blue in 30% methanol (Fig. 2 H and Fig. S3 A). Invading sprouts were visualized using an Olympus BX51 inverted microscope under transmitted light using UPlan FLN 10× objective (NA 0.3; for quantification, Fig. 2 I and Fig. S3 A) or 20× Plan N objective (NA 0.4; for side view images of sprouts, Fig. 2 H). Sprouts were counted in two to four fields per well and averaged over a minimum of three wells per condition. Sprout formation data are expressed as mean number of invading sprouts per well ± standard error (SE) with each data point representing one well. Data were collected from three independent experiments (Fig. 2 I). The additional invasion assay depicted in Fig. 2, F and G, was prepared the same way using untreated ECs. Cells were coimmunostained after fixation with Septin2 (Cat# HPA018481; Sigma-Aldrich) and MT1-MMP (Cat# MAB3328; Millipore) to localize Septin2 with podosome activity in invading sprouts (Fig. 2 F). Imaris Image Analysis software was used to create a representative 3D surface rendering of ECs invading into 3D collagen matrix (Fig. 2 G).

Quantification of focal adhesions

Aptitude for focal adhesion formation was compared in cells with downregulated Septin2 expression versus scramble control cells. Septin2 expression was downregulated using two individual siRNA, each targeting SEPT2 applied 48 h before cells being seeded onto glass-bottom dishes previously coated in 0.2%

gelatin and 5 mg/ml fibronectin. Cells were fixed and stained for focal adhesions using FAK antibody (Cat# 610087; BD PharMingen) 24 h after plating. Cells were imaged in total internal reflection fluorescence (TIRF) using an Olympus IX-83 microscope with PlanApo N 60× TIRF microscope objective (oil, NA 1.45) and a 561-nm laser line. Images were analyzed using data collected from 10 fields of view per condition over a total of three independent experiments. Focal adhesions were quantified using ImageJ analysis software. Each image was thresholded the same way using equal background subtraction. "Find local maxima" function was then used to quantify focal adhesions. The total number of focal adhesions was normalized to cell surface area using MetaMorph Image Analysis software to manually outline cell border and subtract from total growth area. Student's *t* tests for pairwise comparison between conditions were used to determine statistical significance. Data are presented as total number of focal adhesions/cell surface area ± SE (Fig. S3 F).

Podosome formation and matrix degradation assays

Fluorescent gelatin–coated coverslips were prepared as previously described (Martin et al., 2012). To coat coverslips, Oregon Green-488-conjugated gelatin was mixed with unlabeled 0.2% gelatin in PBS at a ratio of 1:8, respectively. Gelatin conjugated to Alexa Fluor 405 was mixed with unlabeled 0.2% gelatin in PBS at a ratio of 1:20, respectively. HPAECs were seeded onto coverslips 6–24 h before RapR-Src stimulation (length of stimulation is indicated in figure legends). Cells were fixed and stained for F-actin using Alexa Fluor 647 phalloidin. At least 10 fields of view per condition were imaged using an Olympus IX-83 widefield microscope with UPlanSAPO 40× silicon oil objective. Only fields with confluent cells (90%–100%) expressing RapR-Src-Cerulean-Myc and mCherry-FRB (adenoviral transduction) were selected for analysis. At least 90 cells per condition were counted over three independent experiments. The functional podosomes were defined as areas where actin focus signal overlapped with quenched fluorescent gelatin signal. The percentage of cells displaying the formation of functional podosomes (podosome phenotype) was quantified in at least 10 fields of view per condition for each independent experiment. A cell forming at least one functional podosome was counted as displaying the podosome phenotype. A two-sample *t* test was used for statistical analysis (as in Fig. 2 B). Total matrix degradation was measured using MetaMorph Image Analysis software. A binary mask of the quenched gelatin signal was used to measure the degradation area in each field of view. Statistical significance was determined using a Student's *t* test for pairwise comparisons between conditions (as in Fig. 5 E; Fig. S1, A and F; and Fig. S2, H and J).

To determine the total number of actin foci, images of HPAECs stained with Alexa Fluor 647 phalloidin were analyzed using the Invadopodia Colocalization Macro for ImageJ analysis software (Fig. 4 A; Sharma et al., 2013b). At least 10 fields of view from five independent experiments were analyzed for each condition. Statistical significance was determined using a Student's *t* test to draw pairwise comparisons between knockdown and scramble control conditions.

Matrix degradation assays were also performed in Fig. 1 E and Fig. S1 A using VEGF stimulation as indicated in the figure legend. Total matrix degradation was quantified, and statistical analysis was performed as described for matrix degradation assays using RapR-Src activation as the stimulus.

Matrix degradation assays performed with MDA-MB-231 cells and BMDM were performed by seeding cells onto Oregon Green-488–conjugated gelatin coverslips for 24 h before fixation and staining with Alexa Fluor 647 phalloidin. Confocal images were acquired using a Zeiss LSM880 Axio Observer with 63× Plan Apochromat oil objective (NA 1.4; Fig. S2, D and E).

Matrix degradation assays were performed in response to Src activation (as previously described) in the presence of specific inhibitors. Cells were pretreated with a specific inhibitor of MT1-MMP (NSC405020, Cat# 444295; Sigma-Aldrich) with a final concentration of 150 µM for 48 h before Src activation. Global MMP inhibitor GM6001 (Cat# CC1000; Sigma-Aldrich) and blebbistatin (Cat# 2406-1; BioVision) were each added to final concentrations of 100 µM and 50 µM, respectively, 0.5 h preceding Src activation. Src was then activated for 0.5 h preceding fixation and staining. Total matrix degradation was quantified as described previously using at least 10 fields of view per condition from a total of three independent experiments.

Image acquisition

Fixed samples

Fixed samples were mounted on glass coverslips using Fluoromount-G and imaged using a confocal, widefield, or high-resolution Airyscan confocal microscopy as indicated in the figure legends. Widefield images were acquired using an Olympus IX-83 microscope using UPlanSAPO 40× silicon oil (NA 1.25; Fig. 2 A and Fig. S4 B) or PlanApo N 60× TIRF microscope objective (oil, NA 1.45; Fig. S2 C). Confocal images were acquired using a Zeiss LSM 710 confocal microscope with 63× Plan Apochromat oil objective (NA 1.4; Fig. 1 A and Fig. S1, D and E), Zeiss LSM 710 META with 63× Alpha Plan Apochromat oil objective (NA 1.46; Fig. 3, D and F), or Zeiss LSM880 Axio Observer with 63× Plan Apochromat oil objective (NA 1.4; Fig. 2 F and Fig. S2, A, B, D, and E). Airyscan confocal imaging was performed using Zeiss LSM 880 AxioObserver confocal microscope with Airyscan detector and 63× Plan Apochromat oil objective (NA 1.4). Images were acquired in superresolution scan mode (Fig. 1, B and E; and Fig. 5, A and B).

Live cell image acquisition

Cells were seeded on glass coverslips coated with 0.2% gelatin and 5 mg/ml fibronectin. Coverslips were mounted in an Attofluor cell chamber (Cat# A78-16; Invitrogen). Cells were imaged at 37°C in EGM-2 media with 10% FBS. Widefield images were acquired using an Olympus IX-83 widefield microscope with UPlanSAPO 40X silicon oil objective (NA 1.25; Fig. 5 D; Fig. S1, B and C; and Video 1). Ring TIRF images were acquired using DeltaVision OMX SR superresolution microscope TIRF illumination module with 60× ApoM TIRF objective (NA 1.49; Fig. 4, B and D).

Membrane proximity of Septin2 within podosomes

HPAECs expressing RapR-Src-as2-Cerulean-Myc and GFP(Y66S)-FRB (adenoviral transduction) and cotransfected with Septin2-

rsTagRFP and integrin β_3-Dronpa were plated onto coverslips coated with 0.2% gelatin and fibronectin (5 mg per liter). RapR-Src was activated for 0.5 h with rapamycin (500 nM). Cells were then fixed and stained with Alexa Fluor 405 phalloidin to label F-actin as a marker for Src-induced podosome formation when colocalized with β_3 integrin. Cells were imaged using a Zeiss LSM 880 AxioObserver confocal microscope with Airyscan detector and 63× Plan Apochromat oil objective (NA 1.4). Images were acquired in superresolution scan mode (Fig. 5, A and B). ImageJ analysis software was used to create Z axial profiles of fluorescence intensity comparing Septin2 with respect to β_3 integrin within the podosome (Fig. 5 C).

Ring TIRF order of arrival analysis

HPAECs were cotransfected pairwise (using Cytofect reagent) with DNA constructs expressing fTractin-iRFP670 and TKS5-GFP or Septin2-TagRFP and TKS5-GFP. All cells were also transduced with adenoviruses expressing RapR-Src-as2-Cerulean-Myc and GFP(Y66S)-FRB 18 h before imaging. Cells were seeded on glass coverslips coated with 0.2% gelatin and fibronectin (5 mg per liter) and mounted in Attofluor chambers and imaged in EGM-2 containing 10% FBS. Live ring TIRF imaging was performed at 5% CO_2 and 37°C using a DeltaVision OMX superresolution microscope TIRF illumination module with 60× ApoM TIRF oil objective (NA 1.49; Fig. 4, B and D). Images were acquired every 10 s for 30 min. Rapamycin (500 nm) was added 15 min before the start of image acquisition. New foci that formed during imaging and exhibited colocalization of Tks5/F-actin or Tks5/Septin2 were identified and analyzed using MetaMorph Image Analysis software. To assess arrival of each protein at the foci, each focus was outlined as a region of interest, and changes in integrated fluorescence intensity within the region were measured over time. To determine the time difference in arrival between podosomal proteins, individual foci were analyzed using Invadopodia Tracker V3 plugin for Fiji image analysis software (Sharma et al., 2013c). The arrival time of F-actin and Septin2 at each focus was determined with respect to arrival of Tks5. Statistical significance was determined using a two-sample *t* test.

Statistical analysis and software

OriginPro software was used to carry out Student's *t* tests for pairwise comparisons in all experiments. Number of replicates and type of statistical comparisons are defined in figure legends as well as throughout the Method details section. For all *t* tests, P values <0.05 were considered to be significant. Statistical data were plotted using OriginPro (method indicated in figure legends). The model in Fig. 5 F was created with BioRender software.

Online supplemental material

Fig. S1 demonstrates the role of Src, metalloproteases, and myosin in the formation of endothelial podosomes and depicts the localization of endogenous Septin2 to Src-induced podosomes. Fig. S2 shows the localization of septins to podosomes and invadopodia in different cell types and demonstrates their role in podosome formation. Fig. S3 shows the role of Septin2 in regulating different functional steps that mediate the invasion of ECs into a 3D matrix and the formation of endothelial sprouts. Fig. S4 demonstrates the requirement for the interaction of Septin2 with PIPs in the regulation of endothelial podosomes (accompanies experiment in Fig. 5 E). Video 1 shows Septin2 localization after Src activation (accompanies Fig. S1, B and C).

Acknowledgments

We are grateful to Dr. Peter Toth and Dr. Ke Ma, director and co-director of the Fluorescence Imaging Core in the Research Resources Center at University of Illinois at Chicago, for help with imaging experiments and training in microscopy techniques and analysis. We thank Ankit Jambusaria for consulting on experimental analysis. We also extend our gratitude to Vincent Huyot for unfailing help with technical training and experimental insights throughout this project. Special thanks to Jordan Fauser for help with data analysis. We also thank Dr. Jan Kitajewski and Dr. Dan Shaye, Department of Physiology and Biophysics, for assistance with Airyscan confocal imaging.

We extend our thanks for funding support from the American Heart Association (17PRE33400022 Predoctoral Fellowship to K.B. Collins and 17SDG33700146 Scientist Development Grant to H. Kang), the Chicago Biomedical Consortium (CBC Pilot Grant to A.V. Karginov), and the US National Institutes of Health (T32 HL007829-22 to A.B. Malik and R21CA159179 to A.V. Karginov).

The authors declare no competing financial interests.

Author Contributions: K.B. Collins and A.V. Karginov initiated the project, and K.B. Collins performed the experiments. H. Kang participated in endothelial sprouting and in vivo angiogenesis experiments and performed the matrix degradation inhibitor experiment. J.E. Klomp and J. Matsche produced reagents for the experiments. J. Matsche assisted with sample preparation and Western blotting. A.V. Karginov, A.B. Malik, and J. Rehman coordinated the study. K.B. Collins, A.V. Karginov, J. Rehman, A.B. Malik, and J.E. Klomp contributed to manuscript preparation.

Submitted: 4 March 2019
Revised: 14 September 2019
Accepted: 8 November 2019

References

Auerbach, R., R. Lewis, B. Shinners, L. Kubai, and N. Akhtar. 2003. Angiogenesis assays: a critical overview. *Clin. Chem.* 49:32–40. https://doi.org/10.1373/49.1.32

Barral, Y., and I.M. Mansuy. 2007. Septins: cellular and functional barriers of neuronal activity. *Curr. Biol.* 17:R961–R963. https://doi.org/10.1016/j.cub.2007.10.001

Bhuwania, R., S. Cornfine, Z. Fang, M. Krüger, E.J. Luna, and S. Linder. 2012. Supervillin couples myosin-dependent contractility to podosomes and enables their turnover. *J. Cell Sci.* 125:2300–2314. https://doi.org/10.1242/jcs.100032

Block, M.R., C. Badowski, A. Millon-Fremillon, D. Bouvard, A.-P. Bouin, E. Faurobert, D. Gerber-Scokaert, E. Planus, and C. Albiges-Rizo. 2008. Podosome-type adhesions and focal adhesions, so alike yet so different. *Eur. J. Cell Biol.* 87:491–506. https://doi.org/10.1016/j.ejcb.2008.02.012

Boateng, L.R., and A. Huttenlocher. 2012. Spatiotemporal regulation of Src and its substrates at invadosomes. *Eur. J. Cell Biol.* 91:878–888. https://doi.org/10.1016/j.ejcb.2012.06.003

Bowen, J.R., D. Hwang, X. Bai, D. Roy, and E.T. Spiliotis. 2011. Septin GTPases spatially guide microtubule organization and plus end dynamics in polarizing epithelia. *J. Cell Biol.* 194:187–197. https://doi.org/10.1083/jcb.201102076

Bridges, A.A., H. Zhang, S.B. Mehta, P. Occhipinti, T. Tani, and A.S. Gladfelter. 2014. Septin assemblies form by diffusion-driven annealing on membranes. *Proc. Natl. Acad. Sci. USA.* 111:2146–2151. https://doi.org/10.1073/pnas.1314138111

Burridge, K., and C. Guilluy. 2016. Focal adhesions, stress fibers and mechanical tension. *Exp. Cell Res.* 343:14–20. https://doi.org/10.1016/j.yexcr.2015.10.029

Carpentier, G. 2012. Angiogenesis Analyzer for ImageJ. Available at: http://image.bio.methods.free.fr/ImageJ/?Angiogenesis-Analyzer-for-ImageJ (accessed February 6, 2018)

Casamayor, A., and M. Snyder. 2003. Molecular dissection of a yeast septin: distinct domains are required for septin interaction, localization, and function. *Mol. Cell. Biol.* 23:2762–2777. https://doi.org/10.1128/MCB.23.8.2762-2777.2003

Chellaiah, M.A. 2006. Regulation of podosomes by integrin alphavbeta3 and Rho GTPase-facilitated phosphoinositide signaling. *Eur. J. Cell Biol.* 85:311–317. https://doi.org/10.1016/j.ejcb.2006.01.008

Cho, J.-A., P. Osenkowski, H. Zhao, S. Kim, M. Toth, K. Cole, A. Aboukameel, A. Saliganan, L. Schuger, R.D. Bonfil, et al. 2008. The inactive 44-kDa processed form of membrane type 1 matrix metalloproteinase (MT1-MMP) enhances proteolytic activity via regulation of endocytosis of active MT1-MMP. *J. Biol. Chem.* 283:17391–17405. https://doi.org/10.1074/jbc.M708943200

Chu, P.-H., D. Tsygankov, M.E. Berginski, O. Dagliyan, S.M. Gomez, T.C. Elston, A.V. Karginov, and K.M. Hahn. 2014. Engineered kinase activation reveals unique morphodynamic phenotypes and associated trafficking for Src family isoforms. *Proc. Natl. Acad. Sci. USA.* 111:12420–12425. https://doi.org/10.1073/pnas.1404487111

Curado, F., P. Spuul, I. Egaña, P. Rottiers, T. Daubon, V. Veillat, P. Duhamel, A. Leclercq, E. Gontier, and E. Génot. 2014. ALK5 and ALK1 play antagonistic roles in transforming growth factor β-induced podosome formation in aortic endothelial cells. *Mol. Cell. Biol.* 34:4389–4403. https://doi.org/10.1128/MCB.01026-14

Damalio, J.C.P., T.M. Nobre, J.L. Lopes, O.N. Oliveira Jr., and A.P.U. Araújo. 2013. Lipid interaction triggering Septin2 to assembly into β-sheet structures investigated by Langmuir monolayers and PM-IRRAS. *Biochim. Biophys. Acta.* 1828:1441–1448. https://doi.org/10.1016/j.bbamem.2013.02.003

Destaing, O., A. Sanjay, C. Itzstein, W.C. Horne, D. Toomre, P. De Camilli, and R. Baron. 2008. The tyrosine kinase activity of c-Src regulates actin dynamics and organization of podosomes in osteoclasts. *Mol. Biol. Cell.* 19:394–404. https://doi.org/10.1091/mbc.e07-03-0227

Destaing, O., S.M. Ferguson, A. Grichine, C. Oddou, P. De Camilli, C. Albiges-Rizo, and R. Baron. 2013. Essential function of dynamin in the invasive properties and actin architecture of v-Src induced podosomes/invadosomes. *PLoS One.* 8:e77956. https://doi.org/10.1371/journal.pone.0077956

Di Martino, J., L. Paysan, C. Gest, V. Lagrée, A. Juin, F. Saltel, and V. Moreau. 2014. Cdc42 and Tks5: a minimal and universal molecular signature for functional invadosomes. *Cell Adhes. Migr.* 8:280–292. https://doi.org/10.4161/cam.28833

El Azzouzi, K., C. Wiesner, and S. Linder. 2016. Metalloproteinase MT1-MMP islets act as memory devices for podosome reemergence. *J. Cell Biol.* 213:109–125. https://doi.org/10.1083/jcb.201510043

Ewers, H., T. Tada, J.D. Petersen, B. Racz, M. Sheng, and D. Choquet. 2014. A Septin-Dependent Diffusion Barrier at Dendritic Spine Necks. *PLoS One.* 9:e113916. https://doi.org/10.1371/journal.pone.0113916

Gawden-Bone, C., M.A. West, V.L. Morrison, A.J. Edgar, S.J. McMillan, B.D. Dill, M. Trost, A. Prescott, S.C. Fagerholm, and C. Watts. 2014. A crucial role for β2 integrins in podosome formation, dynamics and Toll-like-receptor-signaled disassembly in dendritic cells. *J. Cell Sci.* 127:4213–4224. https://doi.org/10.1242/jcs.151167

Genna, A., S. Lapetina, N. Lukic, S. Twafra, T. Meirson, V.P. Sharma, J.S. Condeelis, and H. Gil-Henn. 2018. Pyk2 and FAK differentially regulate invadopodia formation and function in breast cancer cells. *J. Cell Biol.* 217:375–395. https://doi.org/10.1083/jcb.201702184

Gilden, J., and M.F. Krummel. 2010. Control of cortical rigidity by the cytoskeleton: emerging roles for septins. *Cytoskeleton (Hoboken).* 67:477–486. https://doi.org/10.1002/cm.20461

Gimona, M., R. Buccione, S.A. Courtneidge, and S. Linder. 2008. Assembly and biological role of podosomes and invadopodia. *Curr. Opin. Cell Biol.* 20:235–241. https://doi.org/10.1016/j.ceb.2008.01.005

Gong, H., M. Liu, J. Klomp, B.J. Merrill, J. Rehman, and A.B. Malik. 2017. Method for Dual Viral Vector Mediated CRISPR-Cas9 Gene Disruption in Primary Human Endothelial Cells. *Sci. Rep.* 7:42127. https://doi.org/10.1038/srep42127

Guo, S., J. Lok, Y. Liu, K. Hayakawa, W. Leung, C. Xing, X. Ji, and E.H. Lo. 2014. Assays to examine endothelial cell migration, tube formation, and gene expression profiles. *Methods Mol. Biol.* 1135:393–402. https://doi.org/10.1007/978-1-4939-0320-7_32

Hall, P.A., K. Jung, K.J. Hillan, and S.E. Russell. 2005. Expression profiling the human septin gene family. *J. Pathol.* 206:269–278. https://doi.org/10.1002/path.1789

Han, Y., K. Yang, A. Proweller, G. Zhou, M.K. Jain, and D.L. Ramirez-Bergeron. 2012. Inhibition of ARNT severely compromises endothelial cell viability and function in response to moderate hypoxia. *Angiogenesis.* 15:409–420. https://doi.org/10.1007/s10456-012-9269-x

Hertel, F., G.C.H. Mo, S. Duwé, P. Dedecker, and J. Zhang. 2016. RefSOFI for Mapping Nanoscale Organization of Protein-Protein Interactions in Living Cells. *Cell Reports.* 14:390–400. https://doi.org/10.1016/j.celrep.2015.12.036

Hoshino, D., J. Jourquin, S.W. Emmons, T. Miller, M. Goldgof, K. Costello, D.R. Tyson, B. Brown, Y. Lu, N.K. Prasad, et al. 2012. Network analysis of the focal adhesion to invadopodia transition identifies a PI3K-PKCα invasive signaling axis. *Sci. Signal.* 5:ra66. https://doi.org/10.1126/scisignal.2002964

Hoshino, D., K.M. Branch, and A.M. Weaver. 2013. Signaling inputs to invadopodia and podosomes. *J. Cell Sci.* 126:2979–2989. https://doi.org/10.1242/jcs.079475

Hu, Q., L. Milenkovic, H. Jin, M.P. Scott, M.V. Nachury, E.T. Spiliotis, and W.J. Nelson. 2010. A septin diffusion barrier at the base of the primary cilium maintains ciliary membrane protein distribution. *Science.* 329:436–439. https://doi.org/10.1126/science.1191054

Joo, E., M.C. Surka, and W.S. Trimble. 2007. Mammalian SEPT2 is required for scaffolding nonmuscle myosin II and its kinases. *Dev. Cell.* 13:677–690. https://doi.org/10.1016/j.devcel.2007.09.001

Kang, H., K.J. Bayless, and R. Kaunas. 2008. Fluid shear stress modulates endothelial cell invasion into three-dimensional collagen matrices. *Am. J. Physiol. Heart Circ. Physiol.* 295:H2087–H2097. https://doi.org/10.1152/ajpheart.00281.2008

Kang, H., Z. Hong, M. Zhong, J. Klomp, K.J. Bayless, D. Mehta, A.V. Karginov, G. Hu, and A.B. Malik. 2019. Piezo1 mediates angiogenesis through activation of MT1-MMP signaling. *Am. J. Physiol. Cell Physiol.* 316:C92–C103. https://doi.org/10.1152/ajpcell.00346.2018

Karginov, A.V., and K.M. Hahn. 2011. Allosteric activation of kinases: Design and application of RapR kinases. *Curr. Protoc. Cell Biol.* 53:14.13.1–14.13.16. https://doi.org/10.1002/0471143030.cb1413s53

Karginov, A.V., F. Ding, P. Kota, N.V. Dokholyan, and K.M. Hahn. 2010. Engineered allosteric activation of kinases in living cells. *Nat. Biotechnol.* 28:743–747. https://doi.org/10.1038/nbt.1639

Karginov, A.V., D. Tsygankov, M. Berginski, P.-H. Chu, E.D. Trudeau, J.J. Yi, S. Gomez, T.C. Elston, and K.M. Hahn. 2014. Dissecting motility signaling through activation of specific Src-effector complexes. *Nat. Chem. Biol.* 10:286–290. https://doi.org/10.1038/nchembio.1477

Kelley, L.C., A.G. Ammer, K.E. Hayes, K.H. Martin, K. Machida, L. Jia, B.J. Mayer, and S.A. Weed. 2010. Oncogenic Src requires a wild-type counterpart to regulate invadopodia maturation. *J. Cell Sci.* 123:3923–3932. https://doi.org/10.1242/jcs.075200

Kim, M.S., C.D. Froese, M.P. Estey, and W.S. Trimble. 2011. SEPT9 occupies the terminal positions in septin octamers and mediates polymerization-dependent functions in abscission. *J. Cell Biol.* 195:815–826. https://doi.org/10.1083/jcb.201106131

Kittaka, M., K. Mayahara, T. Mukai, T. Yoshimoto, T. Yoshitaka, J.P. Gorski, and Y. Ueki. 2018. Cherubism mice also deficient in c-Fos exhibit inflammatory bone destruction executed by macrophages that express MMP14 despite the absence of TRAP+ osteoclasts. *J. Bone Miner. Res.* 33:167–181. https://doi.org/10.1002/jbmr.3295

Klomp, J.E., V. Huyot, A.-M. Ray, K.B. Collins, A.B. Malik, and A.V. Karginov. 2016. Mimicking transient activation of protein kinases in living cells. *Proc. Natl. Acad. Sci. USA.* 113:14976–14981. https://doi.org/10.1073/pnas.1609675114

Klomp, J.E., M. Shaaya, J. Matsche, R. Rebiai, J.S. Aaron, K.B. Collins, V. Huyot, A.M. Gonzalez, W.A. Muller, T.-L. Chew, et al. 2019. Time-Variant SRC Kinase Activation Determines Endothelial Permeability Response. *Cell Chem. Biol.* 26:1081–1094.e6: E6. https://doi.org/10.1016/j.chembiol.2019.04.007

Kwak, H.-I., H. Kang, J.M. Dave, E.A. Mendoza, S.-C. Su, S.A. Maxwell, and K.J. Bayless. 2012. Calpain-mediated vimentin cleavage occurs upstream of MT1-MMP membrane translocation to facilitate endothelial sprout initiation. *Angiogenesis.* 15:287–303. https://doi.org/10.1007/s10456-012-9262-4

Liang, C.-C., A.Y. Park, and J.-L. Guan. 2007. In vitro scratch assay: a convenient and inexpensive method for analysis of cell migration in vitro. *Nat. Protoc.* 2:329–333. https://doi.org/10.1038/nprot.2007.30

Linder, S., and C. Wiesner. 2016. Feel the force: Podosomes in mechanosensing. *Exp. Cell Res.* 343:67–72. https://doi.org/10.1016/j.yexcr.2015.11.026

Low, C., and I.G. Macara. 2006. Structural analysis of septin 2, 6, and 7 complexes. *J. Biol. Chem.* 281:30697–30706. https://doi.org/10.1074/jbc.M605179200

Luxenburg, C., S. Winograd-Katz, L. Addadi, and B. Geiger. 2012. Involvement of actin polymerization in podosome dynamics. *J. Cell Sci.* 125:1666–1672. https://doi.org/10.1242/jcs.075903

Marsboom, G., G.-F. Zhang, N. Pohl-Avila, Y. Zhang, Y. Yuan, H. Kang, B. Hao, H. Brunengraber, A.B. Malik, and J. Rehman. 2016. Glutamine Metabolism Regulates the Pluripotency Transcription Factor OCT4. *Cell Reports.* 16:323–332. https://doi.org/10.1016/j.celrep.2016.05.089

Martin, K.H., K.E. Hayes, E.L. Walk, A.G. Ammer, S.M. Markwell, and S.A. Weed. 2012. Quantitative Measurement of Invadopodia-mediated Extracellular Matrix Proteolysis in Single and Multicellular Contexts. *J. Vis. Exp.* (66). https://doi.org/10.3791/4119

Meddens, M.B.M., E. Pandzic, J.A. Slotman, D. Guillet, B. Joosten, S. Mennens, L.M. Paardekooper, A.B. Houtsmuller, K. van den Dries, P.W. Wiseman, et al. 2016. Actomyosin-dependent dynamic spatial patterns of cytoskeletal components drive mesoscale podosome organization. *Nat. Commun.* 7:13127. https://doi.org/10.1038/ncomms13127

Murphy, D.A., and S.A. Courtneidge. 2011. The 'ins' and 'outs' of podosomes and invadopodia: characteristics, formation and function. *Nat. Rev. Mol. Cell Biol.* 12:413–426. https://doi.org/10.1038/nrm3141

Neubauer, K., and B. Zieger. 2017. The Mammalian Septin Interactome. *Front. Cell Dev. Biol.* 5:3. https://doi.org/10.3389/fcell.2017.00003

Oikawa, T., T. Itoh, and T. Takenawa. 2008. Sequential signals toward podosome formation in NIH-src cells. *J. Cell Biol.* 182:157–169. https://doi.org/10.1083/jcb.200801042

Osiak, A.-E., G. Zenner, and S. Linder. 2005. Subconfluent endothelial cells form podosomes downstream of cytokine and RhoGTPase signaling. *Exp. Cell Res.* 307:342–353. https://doi.org/10.1016/j.yexcr.2005.03.035

Peng, X.-R., Z. Jia, Y. Zhang, J. Ware, and W.S. Trimble. 2002. The septin CDCrel-1 is dispensable for normal development and neurotransmitter release. *Mol. Cell. Biol.* 22:378–387. https://doi.org/10.1128/MCB.22.1.378-387.2002

Potente, M., H. Gerhardt, and P. Carmeliet. 2011. Basic and therapeutic aspects of angiogenesis. *Cell.* 146:873–887. https://doi.org/10.1016/j.cell.2011.08.039

Rowland, M.M., D. Gong, H.E. Bostic, N. Lucas, W. Cho, and M.D. Best. 2012. Microarray analysis of Akt PH domain binding employing synthetic biotinylated analogs of all seven phosphoinositide headgroup isomers. *Chem. Phys. Lipids.* 165:207–215. https://doi.org/10.1016/j.chemphyslip.2011.12.001

Schell, M.J., C. Erneux, and R.F. Irvine. 2001. Inositol 1,4,5-trisphosphate 3-kinase A associates with F-actin and dendritic spines via its N terminus. *J. Biol. Chem.* 276:37537–37546. https://doi.org/10.1074/jbc.M104101200

Schmidt, K., and B.J. Nichols. 2004. Functional interdependence between septin and actin cytoskeleton. *BMC Cell Biol.* 5:43. https://doi.org/10.1186/1471-2121-5-43

Schoumacher, M., R.D. Goldman, D. Louvard, and D.M. Vignjevic. 2010. Actin, microtubules, and vimentin intermediate filaments cooperate for elongation of invadopodia. *J. Cell Biol.* 189:541–556. https://doi.org/10.1083/jcb.200909113

Seals, D.F., E.F. Azucena Jr., I. Pass, L. Tesfay, R. Gordon, M. Woodrow, J.H. Resau, and S.A. Courtneidge. 2005. The adaptor protein Tks5/Fish is required for podosome formation and function, and for the protease-driven invasion of cancer cells. *Cancer Cell.* 7:155–165. https://doi.org/10.1016/j.ccr.2005.01.006

Seano, G., G. Chiaverina, P.A. Gagliardi, L. di Blasio, A. Puliafito, C. Bouvard, R. Sessa, G. Tarone, L. Sorokin, D. Helley, et al. 2014. Endothelial podosome rosettes regulate vascular branching in tumour angiogenesis. *Nat. Cell Biol.* 16:931–941. https://doi.org/10.1038/ncb3036

Sharma, S., A. Quintana, G.M. Findlay, M. Mettlen, B. Baust, M. Jain, R. Nilsson, A. Rao, and P.G. Hogan. 2013a. An siRNA screen for NFAT activation identifies septins as coordinators of store-operated Ca2+ entry. *Nature.* 499:238–242. https://doi.org/10.1038/nature12229

Sharma, V.P., R. Eddy, D. Entenberg, M. Kai, F.B. Gertler, and J. Condeelis. 2013b. Tks5 and SHIP2 regulate invadopodium maturation, but not initiation, in breast carcinoma cells. *Curr. Biol.* 23:2079–2089. https://doi.org/10.1016/j.cub.2013.08.044

Sharma, V.P., D. Entenberg, and J. Condeelis. 2013c. High-resolution live-cell imaging and time-lapse microscopy of invadopodium dynamics and tracking analysis. *Methods Mol. Biol.* 1046:343–357. https://doi.org/10.1007/978-1-62703-538-5_21

Sheffield, P.J., C.J. Oliver, B.E. Kremer, S. Sheng, Z. Shao, and I.G. Macara. 2003. Borg/septin interactions and the assembly of mammalian septin heterodimers, trimers, and filaments. *J. Biol. Chem.* 278:3483–3488. https://doi.org/10.1074/jbc.M209701200

Sirajuddin, M., M. Farkasovsky, F. Hauer, D. Kühlmann, I.G. Macara, M. Weyand, H. Stark, and A. Wittinghofer. 2007. Structural insight into filament formation by mammalian septins. *Nature.* 449:311–315. https://doi.org/10.1038/nature06052

Soroor, F., M.S. Kim, O. Palander, Y. Balachandran, R. Collins, S. Benlekbir, J. Rubinstein, and W.S. Trimble. 2019. Revised subunit order of mammalian septin complexes explains their in vitro polymerization properties. BioRxiv. doi:https://doi.org/10.1101/569871. (Preprint posted March 07, 2019)

Spiliotis, E.T. 2018. Spatial effects - site-specific regulation of actin and microtubule organization by septin GTPases. *J. Cell Sci.* 131:jcs207555. https://doi.org/10.1242/jcs.207555

Spiliotis, E.T., S.J. Hunt, Q. Hu, M. Kinoshita, and W.J. Nelson. 2008. Epithelial polarity requires septin coupling of vesicle transport to polyglutamylated microtubules. *J. Cell Biol.* 180:295–303. https://doi.org/10.1083/jcb.200710039

Spuul, P., T. Daubon, B. Pitter, F. Alonso, I. Fremaux, I. Kramer, E. Montanez, and E. Génot. 2016. VEGF-A/Notch-Induced Podosomes Proteolyse Basement Membrane Collagen-IV during Retinal Sprouting Angiogenesis. *Cell Reports.* 17:484–500. https://doi.org/10.1016/j.celrep.2016.09.016

Symons, M. 2008. Cell biology: watching the first steps of podosome formation. *Curr. Biol.* 18:R925–R927. https://doi.org/10.1016/j.cub.2008.08.034

van den Dries, K., M.B.M. Meddens, S. de Keijzer, S. Shekhar, V. Subramaniam, C.G. Figdor, and A. Cambi. 2013a. Interplay between myosin IIA-mediated contractility and actin network integrity orchestrates podosome composition and oscillations. *Nat. Commun.* 4:1412. https://doi.org/10.1038/ncomms2402

van den Dries, K., S.L. Schwartz, J. Byars, M.B.M. Meddens, M. Bolomini-Vittori, D.S. Lidke, C.G. Figdor, K.A. Lidke, and A. Cambi. 2013b. Dual-color superresolution microscopy reveals nanoscale organization of mechanosensory podosomes. *Mol. Biol. Cell.* 24:2112–2123. https://doi.org/10.1091/mbc.e12-12-0856

Varon, C., F. Tatin, V. Moreau, E. Van Obberghen-Schilling, S. Fernandez-Sauze, E. Reuzeau, I. Kramer, and E. Génot. 2006. Transforming growth factor β induces rosettes of podosomes in primary aortic endothelial cells. *Mol. Cell. Biol.* 26:3582–3594. https://doi.org/10.1128/MCB.26.9.3582-3594.2006

Wang, J., Y. Taba, J. Pang, G. Yin, C. Yan, and B.C. Berk. 2009. GIT1 mediates VEGF-induced podosome formation in endothelial cells: critical role for PLCgamma. *Arterioscler. Thromb. Vasc. Biol.* 29:202–208. https://doi.org/10.1161/ATVBAHA.108.174391

Wang, Z., X. Liang, M. Cai, and G. Du. 2016. Analysis of invadopodia formation in breast cancer cells. *Methods Mol. Biol.* 1406:203–210. https://doi.org/10.1007/978-1-4939-3444-7_18

Wiesner, C., J. Faix, M. Himmel, F. Bentzien, and S. Linder. 2010. KIF5B and KIF3A/KIF3B kinesins drive MT1-MMP surface exposure, CD44 shedding, and extracellular matrix degradation in primary macrophages. *Blood.* 116:1559–1569. https://doi.org/10.1182/blood-2009-12-257089

Zander, S., S. Baumann, S. Weidtkamp-Peters, and M. Feldbrügge. 2016. Endosomal assembly and transport of heteromeric septin complexes promote septin cytoskeleton formation. *J. Cell Sci.* 129:2778–2792. https://doi.org/10.1242/jcs.182824

Zhang, J., C. Kong, H. Xie, P.S. McPherson, S. Grinstein, and W.S. Trimble. 1999. Phosphatidylinositol polyphosphate binding to the mammalian septin H5 is modulated by GTP. *Curr. Biol.* 9:1458–1467. https://doi.org/10.1016/S0960-9822(00)80115-3